Hypoxia-induced exosomal CAMTA1 promotes radio-resistance in MDA-MB-231 cells by regulating NRG1 to mediate M2 macrophage polarization

QIAN LI[1], MINGHUA JIANG[1], BIQING ZHU[1], WEI WEI[2], LEI XIA[3], JIAN HUANG[1], HAN GAO[1] and MINGYU DU[1]

[1]Department of Radiation Oncology, Jiangsu Cancer Hospital and Jiangsu Institute of Cancer Research and The Affiliated Cancer Hospital of Nanjing Medical University, Nanjing, Jiangsu 210009, P.R. China; [2]Department of General Surgery, Jiangsu Cancer Hospital and Jiangsu Institute of Cancer Research and The Affiliated Cancer Hospital of Nanjing Medical University, Nanjing, Jiangsu 210009, P.R. China; [3]Department of Pathology, Jiangsu Cancer Hospital and Jiangsu Institute of Cancer Research and The Affiliated Cancer Hospital of Nanjing Medical University, Nanjing, Jiangsu 210009, P.R. China

Received July 1, 2025; Accepted December 9, 2025

DOI: 10.3892/ijo.2026.5875

Abstract. Radiotherapy remains an irreplaceable treatment modality for breast cancer (BC). Calmodulin-binding Transcription Activator 1 (CAMTA1) has been implicated in tumor progression; however, its role in BC is unclear. The present study aimed to elucidate the mechanistic function of CAMTA1 in BC. RNA sequencing was performed on RAW264.7 macrophages co-cultured with 4T1 cells and subjected to X-ray irradiation. *In vitro*, THP-1 cells were co-cultured with MDA-MB-231 cells under hypoxic conditions. Exosome morphology was observed under transmission electron microscopy and PKH67 staining was used to trace exosome uptake. Flow cytometry was used to detect CD163 expression while ELISA measured the levels of IL-10 and IL-12. Reverse transcription-quantitative (RT-q) PCR and immunoblotting analysis were used to detect the expressions of neuregulin 1 (NRG1), CAMTA1 and hypoxia-inducible factor-1α. Cell apoptosis, cell cycle distribution, cell viability and proliferation were evaluated using flow cytometry, MTT assay and colony formation assay. *In vivo*, transfected MDA-MB-231 cells were injected into BALB/c nude mice combined with radiotherapy and exosome injection. Histopathological changes in tumor tissues were examined using H&E staining. Immunohistochemistry analysis was performed to assess the expressions of NRG1, Caspase-3 and CD163. RNA sequencing, RT-qPCR and immunoblotting analysis revealed that NRG1 expression was markedly increased in RAW264.7 macrophages co-cultured with 4T1 cells. NRG1 was found to be involved in M2 polarization induced by hypoxia-treated MDA-MB-231 cells, which in turn promoted radio-resistance. CAMTA1 expression was highly expressed in exosomes derived from hypoxic MDA-MB-231 cells and exosomal CAMTA1 promoted the M2 polarization of THP-1 macrophages. *In vivo*, CAMTA1 overexpression greatly enhanced tumor growth, increased NRG1 expression, inhibited cell apoptosis and promoted M2 polarization of macrophages in tumor tissue. MDA-MB-231 cells were found to deliver CAMTA1 to macrophages via exosomes, leading to upregulation of NRG1 and induction of M2 polarization, thereby enhancing BC cells resistance to radiotherapy. These findings provided novel insights into the mechanisms underlying radio-resistance in BC and identify exosomal CAMTA1 as a potential therapeutic target.

Introduction

Breast cancer (BC) is one of the most prevalent malignancies and a leading cause of cancer-related death worldwide, with incidence rates continuing to rise (1,2). Current treatment strategies, including surgery, chemotherapy and radiotherapy (3), have markedly improved patient outcomes. However, individuals with more aggressive or advanced disease often develop resistance to these conventional therapies (4). This underscores an urgent need to identify novel therapeutic targets to overcome radio-resistance in BC.

Tumor-associated macrophages, known for their functional diversity and plasticity, are key components of the BC tumor microenvironment and play crucial roles in disease progression and therapeutic response (5). Under different conditions, macrophages can polarize into either the pro-inflammatory, anti-tumorigenic M1 phenotype or the anti-inflammatory, pro-tumorigenic M2 phenotype. M1 macrophages mediate anti-tumor immunity, whereas M2 macrophages facilitate

Correspondence to: Dr Qian Li, Department of Radiation Oncology, Jiangsu Cancer Hospital and Jiangsu Institute of Cancer Research and The Affiliated Cancer Hospital of Nanjing Medical University, Kunlun Road, 42 Baizi Ting, Xuwu, Nanjing, Jiangsu 210009, P.R. China
E-mail: liqianjch@uic-edu.cn

Key words: breast cancer, Calmodulin-binding transcription activator 1, neuregulin 1, radio-resistance, M2 macrophage

tissue remodeling and tumor progression (6). Notably, the suppression of M2 macrophage polarization has been shown to mitigate radio-resistance in inflammatory BC (7).

Calmodulin-binding transcriptional activators (CAMTAs) are an evolutionarily conserved family of transcription regulatory genes (8). Among them, CAMTA1 is predominantly expressed in neuronal tissues (9). Reduced CAMTA1 expression is associated with unfavorable tumor biomarkers and poor prognosis in several cancers (10). Emerging evidence suggests that CAMTA1 plays an important role in tumor progression. For instance, CAMTA1 expression is reduced in colorectal cancer (CRC) tissues and the silence of CAMTA1 renders CRC cells resistant to oxaliplatin treatment (11). Notably, CAMTA1 expression appears to be elevated in BC tissues, yet its functional role in BC progression remains poorly defined.

Neuregulin 1 (NRG1), a member of the neuregulin family, is widely recognized as an oncogene in multiple cancers and plays critical roles in tumor progression (12,13). For example, NRG1 elevation is associated with aggressive clinical manifestations and acts as a prognostic biomarker in gastric cancer (14). Importantly, increased NRG1 expression has also been reported in BC tissues and cells (15). Bioinformatics analyses reveal a positive correlation between CAMTA1 and NRG1 expression in BC tissues. According to the analysis on GEPIA database (http://gepia2.cancer-pku.cn/), NRG1 expression was positively associated with the M2 macrophage marker CD163. These findings led the present study to propose a novel regulatory mechanism whereby CAMTA1 promotes radio-resistance by facilitating M2 macrophage polarization through NRG1 signaling. This CAMTA1-NRG1-M2 axis, to the best of the authors' knowledge, has not been previously reported and represents a key novelty of the present study.

Accordingly, the present study aimed to investigate the role of CAMTA1 in BC radio-resistance and to explore whether CAMTA1 regulates M2 macrophage polarization via NRG1, thereby providing a potential therapeutic target for improving BC treatment outcomes.

Material and methods

Cell culture and hypoxia treatment. The human BC cell line MDA-MB-231 (cat. no. iCell-h133), the mouse BC 4T1 cells (cat. no. iCell-m067), mouse RAW264.7 macrophages (cat. no. iCell-m047) and human monocytic leukemia THP-1 cells (cat. no. iCell-h213) were obtained from iCell Bioscience Inc. All cells were cultured in RPMI-1640 medium supplemented with 10% FBS (Gibco; Thermo Fisher Scientific, Inc.; cat. no. 10099-14) and 1% penicillin-streptomycin at 37˚C with 5% CO_2. THP-1 cells were differentiated into macrophages through the treatment with 100 ng/ml PMA (16). To induce M2 macrophage polarization, THP-1-derived macrophages were stimulated with 20 ng/ml IL-4 for 36 h (17).

For co-culture experiments, RAW264.7 macrophages and 4T1 cells were seeded into a Transwell chamber with 0.4 μm pore. For next-generation RNA sequencing analysis, RAW264.7 macrophages were subjected to high-energy X-ray irradiation.

For hypoxic treatment and exosome isolation, MDA-MB-231 cells were incubated in a tri-gas incubator of 1% O_2, 5% CO_2 and 94% N_2 with contained exosome-depleted FBS medium for 12 or 24 h, followed by co-culture with THP-1-derived macrophages for 24 h (18). To inhibit exosome biogenesis, MDA-MB-231 cells were pretreated with 10 μM GW4869 prior to further experimentation (19). To further confirm the role of NRG1 in modulating M2 polarization, an anti-NRG1 blocking antibody (10 μg/ml; Ab-2, LabVision) was used for cell treatment (20).

Cell transfection. The pc-DNA3.1 vectors containing the complete sequence of NRG1 (Ov-NRG1), an empty vector (Ov-NC), the small interfering RNA targeting NRG1 (si-NRG1) and the corresponding negative control (si-NC) were purchased from Shanghai GenePharma Co., Ltd. and transfected into THP-1-derived macrophages. The sequences were: si-NRG1#1: 5'-CCCGATTGAAAGAGATGAAAA GC-3'; si-NRG1#2: 5'-TGGGAATGAATTGAATCGAAA AA-3'; si-NRG1#3: 5'-TGGCTGATTCTGGAGAGTATA TG-3'; si-NC: 5'-AAGACAUUGUGUGUCCGCCTT-3'.

The pc-DNA3.1 vectors containing the complete sequence of CAMTA1 (Ov-CAMTA1), the empty vector (Ov-NC), the short hairpin RNA targeting CAMTA1 (sh-CAMTA1) and the corresponding negative control (sh-NC) were obtained from Shanghai GenePharma Co., Ltd. and transfected into MDA-MB-231 cells. The target sequences were: sh-CAMTA1#1: 5'-TGAGGAAATTGCGGCTTATTT-3'; sh-CAMTA1#2: 5'-CCCGACTGTTTCCTCAATAAT-3'; sh-CAMTA1#3: 5'-TCGGTCTGAACCCTCTAATTA-3'; sh-NC: 5'-GGAATCTCATTCGATGCATAC-3'.

Cell transfection was performed using Lipofectamine® 2000 reagent (Invitrogen; Thermo Fisher Scientific, Inc.) according to the manufacturer's instructions.

Exosome isolation and fluorescent labeling. Exosomes were isolated using a standard differential centrifugation protocol. Initially, the conditioned medium was centrifuged at 300 x g for 10 min at 4˚C to remove cell debris, 2,000 x g for 20 min at 4˚C to remove the dead cells and 30 min at 10,000 x g at 4˚C to further remove cell debris (21). The pellet of exosomes was collected through the ultracentrifugation at 100,000 x g for 70 min at 4˚C (22). The exosome particle size was determined by nanoparticle tracking analysis using ZetaView PMX 110 (Particle Metrix).

For fluorescent labeling, purified exosomes were stained with PKH26 red fluorescent labeling kits (MilliporeSigma) according to the manufacturer's instructions. Briefly, ultracentrifuged exosomes were re-suspended in diluent C (100 μl) after ultracentrifugation at 100,000 x g for 70 min at 4˚C and then incubated with PKH26 dye solution (100 μl) at room temperature for 5 min, followed by the addition of 200 μl serum. Subsequently, the labeled exosomes were washed by PBS at 4˚C and then incubated with MDA-MB-231 cells. Fluorescence microscopy was used to visualize exosome uptake.

Transmission electron microscopy. Exosomes were fixed with 2.5% glutaraldehyde at 4˚C, placed onto the copper grids and negatively stained with 2% phosphotungstic acid for 2 min at room temperature. After air-drying, the samples were observed using a transmission electron microscope. Images were analyzed using ImageJ software (version 1.53, National Institutes of Health).

Reverse transcription-quantitative (RT-q) PCR. Total RNA was extracted from sample cells seeded at a density of $1x10^6$ cells per well using TRIzol® reagent (Invitrogen; Thermo Fisher Scientific, Inc.) strictly according to the manufacturer's protocol. 1 μg of RNA was reverse-transcribed into cDNA using a commercial RevertAid cDNA Synthesis kit (Thermo Fisher Scientific, Inc.) according to the manufacturer's instructions. The reverse transcription was performed at 42˚C for 60 min, followed by 70˚C for 5 min to inactivate the reverse transcriptase. qPCR was conducted using SYBR Green PCR Master Mix on the 7500 Fast Real-time PCR system according to the manufacturer's instructions. Thermocycling conditions were as follows: Initial denaturation at 95˚C for 2 min. Denaturation at 94˚C for 15 sec, annealing and extension at 60˚C for 30 sec, 40 cycles. The relative gene expression was determined using $2^{-\Delta\Delta Cq}$ method (23). GAPDH was used as the internal reference gene. All RT-qPCR experiments were performed with three independent biological replicates. The following were the primer sequences: NRG1 (human) forward, 5'-GATTCC TACCGAGACTCTCCTC-3' and reverse, 5'-TGGAAGGCA TGGACACCGTCAT-3'; NRG1 (mouse) forward, 5'-GCTCAT CACTCCACGACTGTCA-3' and reverse, 5'-TGCCTGCTG TTCTCTACCGATG-3'; CAMTA1 (human) forward, 5'-AGT GCAGAAAATGAAGAATGCG-3' and reverse 5'-CAAAAT TCTCCTGCTTGATTCG-3'; CAMTA1 (mouse) forward, 5'-CGGTGGTGTTTGAGTACAAGGC-3' and reverse 5'-CCT CCTTTCCATCTGCTCCAGA-3'; GAPDH (human) forward, 5'-GAAGGTGAAGGTCGGAGTC-3' and reverse, 5'-GAA GATGGTGATGGGATTTC-3', or GAPDH (mouse) forward, 5'-AGGTCGGTGTGAACGGATTTG-3' and reverse, 5'-TGT AGACCATGTAGTTGAGGTCA-3'.

Immunoblotting analysis. The total proteins were extracted from sample cells using RIPA lysis buffer (Beyotime Biotechnology, China) and the protein concentration was quantified using BCA assay kits (Thermo Fisher Scientific, Inc.) according to the manufacturer's instructions. Separated by 10% SDS-PAGE, equal amounts of protein (30 μg per lane) were transferred to PVDF membranes (MilliporeSigma). Blocked by 5% BSA (MilliporeSigma) for 1 h at room temperature, the membranes were incubated with primary antibodies against NRG1 (cat. no. 10527-1-AP; 1:1,000; Proteintech Group, Inc.), hypoxia-inducible factor-1α (HIF-1α; cat. no. 20960-1-AP; 1:2,000; Proteintech Group, Inc.), CD63 (cat. no. 25682-1-AP; 1:2,000; Proteintech Group, Inc.), CD81 (cat. no. 27855-1-AP; 1:1,000; Proteintech Group, Inc.), CD9 (cat. no. 20597-1-AP; 1:2,000; Proteintech Group, Inc.), ALIX (cat. no. 12422-1-AP; 1:5,000; Proteintech Group, Inc.) and GAPDH (cat. no. 10494-1-AP; 1:5,000; Proteintech Group, Inc.) overnight at 4˚C. On the next day, the membranes were incubated with goat anti-rabbit horseradish peroxidase (HRP)-conjugated secondary antibodies (cat. no. SA00001-2; Proteintech Group, Inc.) at room temperature for 3 h. The protein bands were visualized using ECL regent (Thermo Fisher Scientific, Inc.) and protein density was semi-quantified via ImageJ software (version 1.53; National Institutes of Health, USA).

Migration assay. For the Transwell migration assay, MDA-MB-231 cells were suspended in serum-free medium (200 μl) and seeded into the upper chamber, while THP-1-derived macrophages were cultured in medium (800 μl) containing 10% FBS in the lower chamber. After 24 h of co-culture, the non-migrated cells were gently removed while the migrated cells were stained by 0.1% crystal violet for 30 min. The migrated cells in five randomly selected non-overlapping fields were observed under a light microscope.

Detection of M2 macrophage marker. The THP-1 macrophages were suspended in pre-cooled PBS and then centrifuged at 200 x g for 5 min at 4˚C (24). After discarding the supernatant, cells were fixed with 0.2 ml of fixation buffer for 5 min at room temperature and then 0.5 ml of the permeabilization wash buffer was added for 5 min at room temperature. Subsequently, the cells were incubated with CD163 antibody (cat. no. 16627; 1:50; Cell Signaling Technology, Inc.) at room temperature for 30 min. A BD FACSCanto II flow cytometer (BD Biosciences) was used to assess CD163 expression and the data analysis was processed using FlowJo software (version 10.8.1; FlowJo LLC; BD Biosciences).

Flow cytometry analysis of the cell cycle and apoptosis. The MDA-MB-231 cells were washed by PBS and centrifuged to remove the supernatant (25). For cell cycle analysis, MDA-MB-231 cells were treated with 50 μl RNase A and 200 μl PI and incubated in the dark at room temperature for 20 min, followed by flow cytometry analysis. For apoptosis analysis, MDA-MB-231 cells were suspended in 500 μl PBS and then incubated with 5 μl Annexin-V-FITC and 5 μl PI in the dark at room temperature for 15 min, followed by flow cytometry analysis. All samples were analyzed using a BD FACSCanto II flow cytometer (BD Biosciences). Data acquisition and analysis were performed using FlowJo software (version 10.8.1; FlowJo LLC; BD Biosciences). The apoptotic rate was calculated as follows: Apoptotic rate (%)=early apoptotic cells (Annexin V^+/PI^-) + late apoptotic cells (Annexin V^+/PI^+).

Colony formation assay and MTT assay. Cell viability was detected using MTT assay and colony formation assay. For MTT detection, cells were incubated with MTT solution, followed by the aspiration of supernatant and the addition of DMSO (100 μl). The optical density was measured at 490 nm using a microplate reader.

For colony formation assays, the colonies were fixed with methanol at room temperature for 15 min and stained by 0.1% crystal violet at room temperature for 20 min. The number of colonies was counted using under a light microscope (magnification, x100). Five randomly selected, non-overlapping fields per well were examined.

ELISA. The supernatant was collected by centrifugation at 2,000 x g for 5 min at 4˚C. The concentrations of IL-10 and IL-12 were detected using ELISA-related IL-10 assay kits and IL-12 assay kits according to the manufacturer's instructions. The optical density was measured at 450 nm using a microplate reader.

Xenograft tumor model. All animal experiments approved by the Animal Ethics Committee of Jiangsu Cancer Hospital

and Jiangsu Institute of Cancer Research and The Affiliated Cancer Hospital of Nanjing Medical University and conducted in compliance with the National Institutes of Health Guide for the Care and Use of Laboratory Animals (approval no. IACUC-20210216-01). A total of 50 female BALB/c nude mice (4-5 weeks old, weighing 18-22 g) were obtained from Beijing Vital River Laboratory Animal Technology Co., Ltd.. Mice were housed under SPF conditions at a controlled temperature of 22±2˚C, relative humidity of 50-60%, and a 12-h light/dark cycle, with free access to food and water. The mice were subcutaneously injected with $1x10^6$ MDA-MB-231 cells transfected with sh-CAMTA1 or Ov-CAMTA1 and then randomly divided into five groups (n=10): PBS, Normoxic exo, Hypoxic exo, Hypoxic exo + Ov-CAMTA1 and Hypoxic exo + sh-CAMTA1 groups. Mice in PBS group received 30 μl PBS, while mice in remaining groups were treated with 30 μg exosomes. Local radiotherapy in the tumors was performed for consecutive 5 days (2 Gy/d). The tumor growth was monitored every week. After five weeks, the mice were sacrificed by intraperitoneal injection of pentobarbital sodium (150 mg/kg). Death was confirmed based on the disappearance of pain response, no response when pressing the toes with hands or forceps and observation of cardiac and respiratory arrest. Tumor tissues were removed, images captured and collected for histological and immunohistochemistry analysis.

Histological analysis. The collected tumor issues were fixed with 10% formalin at room temperature for 24 h. After fixation, tissues were dehydrated through a graded ethanol series, cleared in xylene, and subsequently embedded in paraffin according to standard protocol. Paraffin-embedded tissues were then sectioned into 7 μm-thick slices. Subsequently, the slices were stained with H&E at room temperature, including hematoxylin staining for 5 min followed by eosin staining for 2 min. The stained sections were observed under a light microscope.

Immunohistochemistry analysis. Immunohistochemistry was performed to assess the expression of NRG1, CD163, and cleaved caspase-3 in tumor tissues. Briefly, antigen retrieval was performed by heating the tissue samples in 1X sodium citrate buffer using a microwave, followed by the incubation with 3% hydrogen peroxide for 10 min and subsequent inhibition with 3% normal goat serum (Solarbio, China) for 1 h at room temperature (26). The slices were then incubated with primary antibody against NRG1 (cat. no. 83323-6-RR; 1:500; Proteintech Group, Inc.), CD163 (cat. no. 83285-4-RR; 1:2,000; Proteintech Group, Inc.) and Caspase-3 (cat. no. 19677-1-AP; 1:500; Proteintech Group, Inc.) overnight at 4˚C. On the next day, the slices were incubated with HRP-labeled secondary antibody (cat. no. ab6721; 1:1,000; Abcam) for 1 h at room temperature. Following the treatment with DAB solution, the counterstaining to hematoxylin was performed for 1 min at room temperature and a light microscope was used for observation.

Public database validation. To explore the expressions of CAMTA1 and NRG1 in BC and validate their association with macrophage polarization, several public databases were used. Gene expression levels of CAMTA1 and NRG1 in The Cancer Genome Atlas-Breast Invasive Carcinoma (TCGA-BRCA) samples were obtained from the UCSC Xena platform (https://xenabrowser.net/). Spearman's correlation between CAMTA1 and NRG1 was analyzed using R software (v4.2.2; https://www.r-project.org/). The correlation between NRG1 expression and M2 macrophage marker CD163 was assessed via the Gene Expression Profiling Interactive Analysis (GEPIA)2 platform (http://gepia2.cancer-pku.cn/) based on TCGA-BRCA tumor data. Kaplan-Meier survival analysis was performed using the KMplot database (https://kmplot.com) with the overall survival in Affymetrix breast cancer cohorts stratified by NRG1 expression.

Statistical analysis. The collected data was processed using GraphPad Prism 8 software (Dotmatics) and presented as mean ± SD. Statistical comparisons between two groups were performed using unpaired Student's t-test (for two groups) while comparisons among three or more groups were conducted using one-way ANOVA with Tukey's test. $P<0.05$ was considered to indicate a statistically significant difference.

Results

NRG1 expression is elevated in RAW264.7 macrophages co-cultured with 4T1 cells. Through next-generation RNA sequencing analysis, NRG1 expression was found to be increased in RAW264.7 macrophages co-cultured with 4T1 cells. By contrast, radiotherapy treatment markedly suppressed NRG1 expression (Fig. 1A). These findings were further confirmed by RT-qPCR and immunoblotting analysis. Compared with the RAW264.7 macrophages group, both the mRNA and protein expressions of NRG1 in RAW264.7 macrophages were markedly increased following the co-culture with 4T1 cells, whereas radiotherapy treatment effectively reversed these changes (Fig. 1B and C).

Hypoxic MDA-MB-231 cells induce the M2 polarization of THP-1 macrophages. Under hypoxic conditions, the protein expression of HIF-1α in MDA-MB-231 cells was assessed using immunoblotting analysis. As shown in Fig. 2A, HIF-1α protein level progressively increased with prolonged hypoxia exposure (0, 12 and 24 h). Based on this observation, MDA-MB-231 cells pre-treated with hypoxia for 24 h were subsequently co-cultured with THP-1-derived macrophages for another 24 h. Following co-culture, the increased HIF-1α expression induced by hypoxia was markedly decreased, yet remained above normoxic control (Fig. 2B). Transwell assays demonstrated that the migration of THP-1 macrophages was markedly increased after co-culture with hypoxia-pretreated MDA-MB-231 cells (Fig. 2C). Flow cytometry analysis further showed that hypoxia stimulation increased the expression of CD163, a well-established M2 macrophage marker, in a time-dependent manner (Fig. 2D and E). IL-12 is a cytokine associated with the M1 phenotype, while IL-10 is indicative of M2 polarization. In addition, ELISA results revealed that hypoxia promoted IL-10 secretion while concomitantly reducing IL-12 production in THP-1 macrophages (Fig. 2F and G). Taken together, these findings suggested that hypoxic MDA-MB-231 cells could facilitate the M2 polarization of THP-1-derived macrophages.

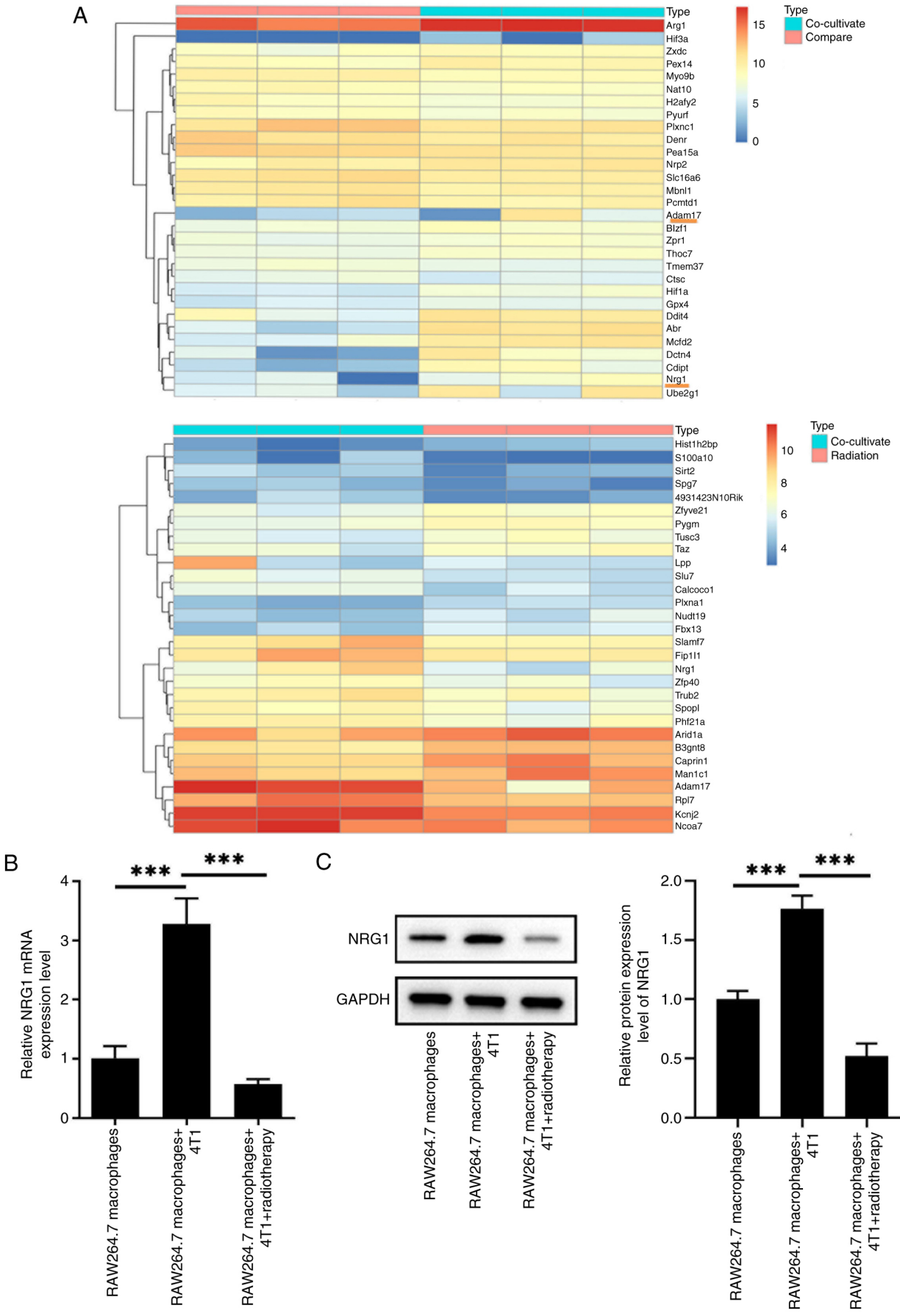

Figure 1. NRG1 expression is elevated in RAW264.7 macrophages co-cultured with 4T1 cells. (A) The expression of NRG1 was examined using next-generation RNA sequencing analysis. (B) The mRNA expression of NRG1 in RAW264.7 macrophages co-cultured with 4T1 cells was detected using reverse transcription-quantitative PCR. (C) The protein expression of NRG1 in RAW264.7 macrophages co-cultured with 4T1 cells was detected using immunoblotting analysis. ***P<0.001. NRG1, neuregulin 1.

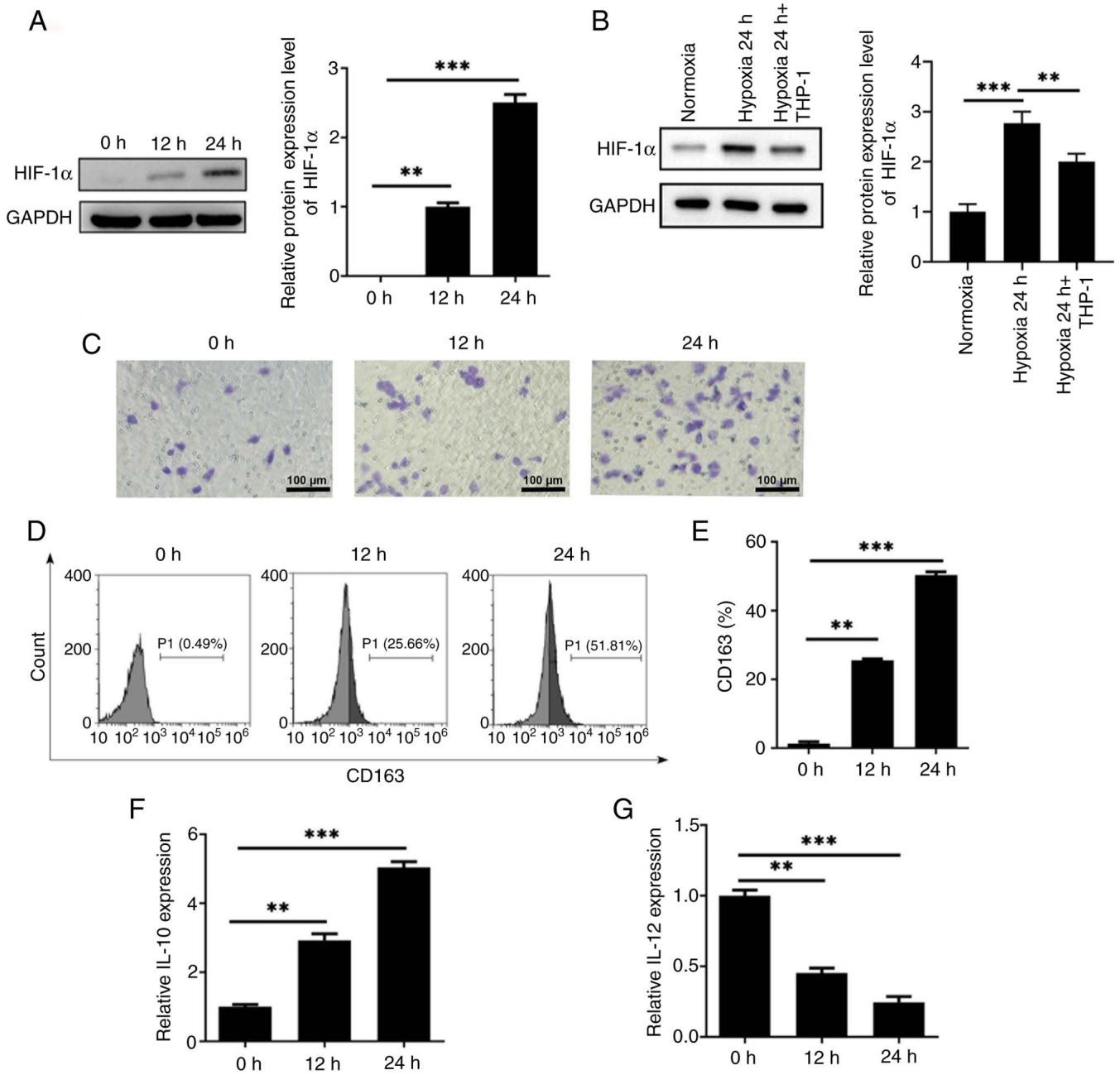

Figure 2. Hypoxic MDA-MB-231 cells induces the M2 polarization of THP-1 macrophages. (A) The protein expression of HIF-1α was assessed using immunoblotting analysis. (B) The protein expression of HIF-1α in hypoxic MDA-MB-231/THP-1 co-cultures was assessed using immunoblotting analysis. (C) The cell migration was detected using Transwell. (D and E) The level of CD163 was detected using flow cytometry. The levels of (F) IL-10 and (G) IL-12 were detected using ELISA-related assay kits. **P<0.01 and ***P<0.001. HIF-1α, hypoxia-inducible factor-1α.

M2 polarization enhances the resistance of MDA-MB-231 cells to radiotherapy. To investigate the radio-resistance of MDA-MB-231 cells, all cells were exposed to X-ray irradiation at doses of 1, 2 and 3 Gy. Given that hypoxic conditions can induce the differentiation of M0 macrophages into M2 macrophages, MDA-MB-231 cells were co-cultured with THP-1 macrophages under hypoxia for varying durations. The cells were divided into MDA-MB-231, MDA-MB-231 + M2, MDA-MB-231 + THP-1 + hypoxia 0 h, MDA-MB-231 + THP-1 + hypoxia 12 h and MDA-MB-231 + THP-1 + hypoxia 24 h groups. MDA-MB-231 cell viability was first assessed using the MTT assay. Compared with the 0 Gy group, MDA-MB-231 cell viability was reduced with increasing radiation dose, whereas co-culture with M2 macrophages conferred the strongest radiation resistance (Fig. 3A). Based on these findings, subsequent experiments were conducted using 2 Gy radiation. Flow cytometry revealed that M2 polarization markedly inhibited the apoptosis of MDA-MB-231 cells. Moreover, hypoxic co-culture with THP-1 macrophages suppressed apoptosis in a time-dependent manner compared with the MDA-MB-231 + THP-1 + hypoxia 0 h group (Fig. 3B and C). To assess whether the reduced apoptosis was associated with altered cell proliferation, cell-cycle distribution was analyzed by flow cytometry. The results showed that M2 polarization markedly increased the proportion of cells in S phase while decreasing the proportion in G_0/G_1 phase,

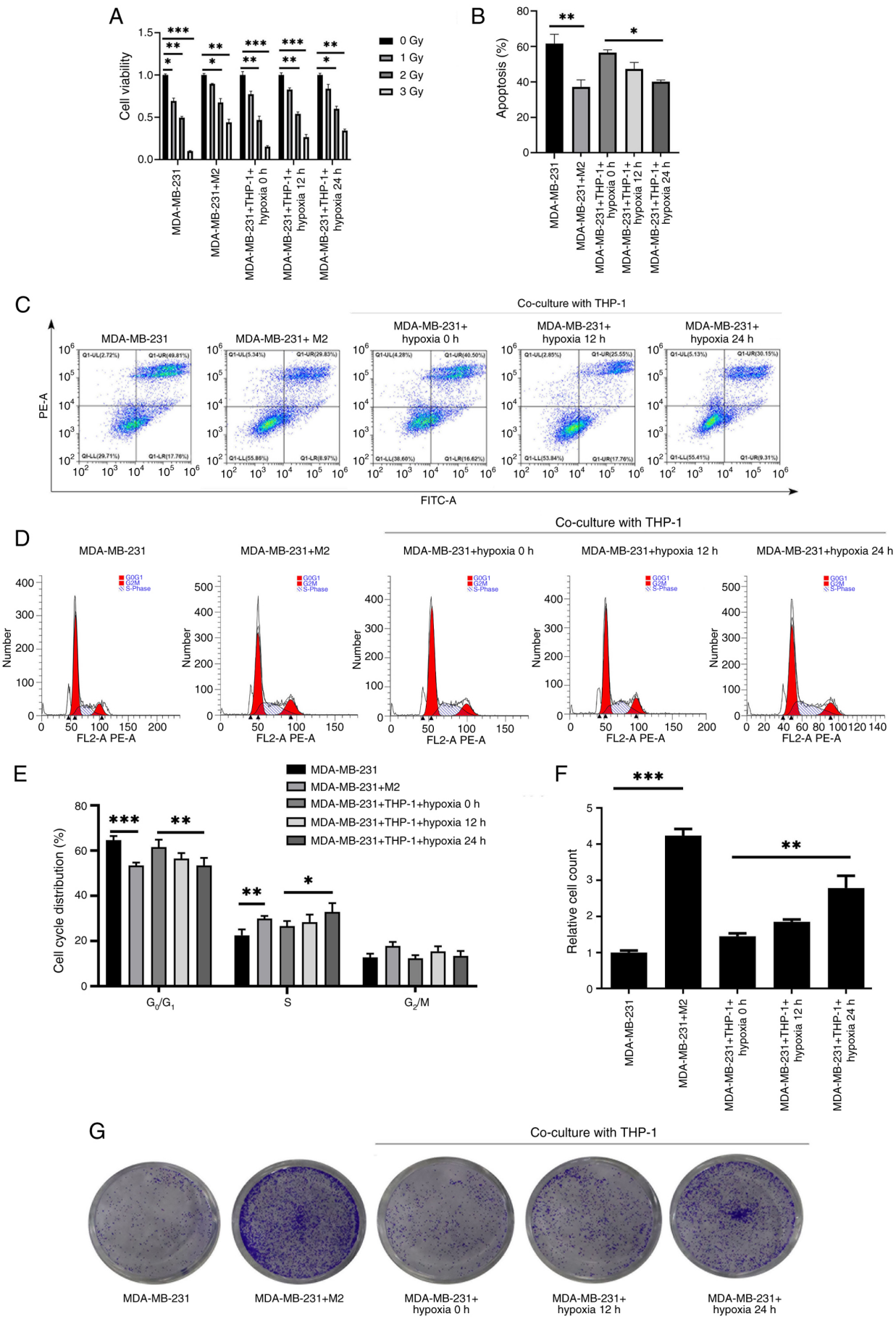

Figure 3. M2 polarization enhances the resistance of MDA-MB-231 cells to radiotherapy. (A) The cell viability was detected using MTT assay. (B and C) The cell apoptosis was detected using flow cytometry. (D and E) The cell cycle was detected using flow cytometry. (F and G) Cell proliferation was detected using colony formation assay. *P<0.05, **P<0.01 and ***P<0.001.

suggesting accelerated DNA synthesis and proliferation potential. Similarly, hypoxic co-culture with THP-1 macrophages increased the S-phase fraction in a time-dependent manner (Fig. 3D and E). In addition, colony formation assays demonstrated that M2 polarization greatly increased the number of colonies compared with the MDA-MB-231 group and hypoxic co-culture with THP-1 macrophages further promoted clonogenic survival (Fig. 3F-G).

NRG1 expression is associated with M2 polarization and poor prognosis. Analysis of the TCGA database revealed that NRG1 expression was markedly upregulated in BC samples (Fig. 4A). GEPIA2 database analysis further demonstrated a positive correlation between NRG1 expression and the M2 macrophage marker CD163 (Fig. 4B). Moreover, Kaplan-Meier survival analysis showed that high NRG1 expression was associated with low overall survival in BC patients (Fig. 4C).

Hypoxic MDA-MB-231 cells induces the M2 polarization of THP-1 macrophages via NRG1. To assess the effects of hypoxia on NRG1 expression, MDA-MB-231 cells were exposed to hypoxia for 24 h and co-cultured with THP-1 macrophages. RT-qPCR analysis revealed that hypoxia markedly upregulated NRG1expression compared with the Normoxia group (Fig. 5A). To upregulate or downregulate NRG1 expression, Ov-NRG1 or si-NRG1 was transfected into cells and the transfection efficacy was examined using RT-qPCR and immunoblotting analysis (Fig. 5B and C). si-NRG1#2 (hereinafter referred as si-NRG1) was selected for subsequent experiments due to its more prominent transfection efficacy. Then, the cells were assigned into M2, M2 + Ov-NRG1, M2 + si-NRG1, Hypoxic MDA-MB-231 + THP-1, Hypoxic MDA-MB-231 + THP-1 + Ov-NRG1 and Hypoxic MDA-MB-231 + THP-1 + si-NRG1 groups. ELISA results showed that Ov-NRG1 elevated IL-10 secretion, whereas si-NRG1 reduced IL-10 level compared with the M2 or Hypoxic MDA-MB-231 + THP-1 groups (Fig. 5D). Consistently, flow cytometry analysis demonstrated that CD163 expression was increased by Ov-NRG1 and decreased by si-NRG1 (Fig. 5E and F). To further verify whether the reduction in IL-10 was specifically attributable to impaired NRG1 signaling, hypoxic MDA-MB-231/THP-1 co-cultures were treated with an anti-NRG1 blocking antibody. Cells were divided into Hypoxic MDA-MB-231 + THP-1, Hypoxic MDA-MB-231 + THP-1 + IgG and Hypoxic MDA-MB-231 + THP-1 + anti-NRG1 antibody groups. Blocking NRG1 markedly decreased IL-10 secretion (Fig. 5G) and consistently reduced CD163 expression (Fig. 5H and I). These findings indicated that hypoxia-induced NRG1 upregulation is a key driver of M2 macrophage polarization, at least in part by enhancing IL-10 secretion and CD163 expression.

Hypoxic MDA-MB-231 cells mediate the M2 polarization of THP-1 macrophages via exosomes. In the tumor microenvironment, macrophages play crucial roles in tumor initiation and progression. To investigate whether exosomes contribute to M2 polarization, MDA-MB-231 cells were treated with the exosome biogenesis inhibitor GW4869 and then co-cultured with THP-1 macrophages. Transwell assays showed that hypoxic MDA-MB-231 cells markedly enhanced the migration of THP-1 macrophages, whereas this effect was notably attenuated by GW4869 treatment (Fig. 6A). Moreover, GW4869 treatment markedly reduced CD163 expression and IL-10 secretion, suggesting that exosomes derived from hypoxic MDA-MB-231 cells are pivotal in promoting M2 polarization (Fig. 6B and C). Transmission electron microscopy further revealed abundant exosomes with typical bilayer membrane structures in the supernatant of hypoxic MDA-MB-231 cells. Nanoparticle size analysis showed that the average exosome diameter was ~100 nm (Fig. 6D and E). Immunoblotting analysis confirmed the presence of exosomal marker proteins CD9, ALIX, CD63 and CD81 in exosome extracts (Fig. 6F).

Exosomes extracted from hypoxic or normoxic MDA-MB-231 cells were subsequently labeled with PKH67 and incubated with THP-1 macrophages. Fluorescence imaging confirmed the successful intake of MDA-MB-231-derived exosomes by THP-1 macrophages (Fig. 6G). Consistently, flow cytometry analysis demonstrated that hypoxia-derived exosomes markedly increased CD163 expression in THP-1 macrophages (Fig. 6H). The above results indicated that hypoxic MDA-MB-231 cells promoted the M2 polarization of THP-1 macrophages via exosomes.

Exosomal CAMTA1 promotes the M2 polarization of THP-1 macrophages. Analysis of the TCGA database revealed that CAMTA1 expression was markedly elevated in BC samples (Fig. 7A). Consistently, RT-qPCR results showed that hypoxic stimulation markedly increased CAMTA1 expression in both MDA-MB-231 cells and their secreted exosomes (Fig. 7B and C). Furthermore, co-culture experiments demonstrated a substantial increase in CAMTA1 expression with recipient THP-1 macrophages after exposure to hypoxia-derived exosomes (Fig. 7D). To reduce CAMTA1 expression, sh-CAMTA1 was transfected into MDA-MB-231 cells and the transfection efficacy was examined using RT-qPCR and immunoblotting analysis (Fig. 7E). sh-CAMTA1#1 (hereinafter referred as sh-CAMTA1) was selected for subsequent experiments due to its improved transfection efficacy. As Fig. 7F and G shows, CAMTA1 expression was markedly reduced in both MDA-MB-231 cells and exosomes following the transfection of sh-CAMTA1. Exosomes from CAMTA1-silenced MDA-MB-231 cells were then incubated with THP-1 macrophages and then divided into Normoxic MDA-MB-231 + exo + sh-NC, Normoxic MDA-MB-231 + exo + sh-CAMTA1, Hypoxic MDA-MB-231 + exo + sh-NC and Hypoxic MDA-MB-231 + exo + sh-CAMTA1 groups. Functional assays revealed that CAMTA1 knockdown markedly impaired the migration of THP-1 macrophages (Fig. 7H). Moreover, CAMTA1 depletion also led to a notable reduction in the expressions of CD163 and IL-10 (Fig. 7I-K).

Exosomal CAMTA1 promotes tumor growth in vivo. To upregulate CAMTA1 expression, Ov-CAMTA1 was transfected into MDA-MB-231 cells and the transfection efficacy was examined (Fig. 8A). To investigate the role of CAMTA1 *in vivo*, MDA-MB-231 cells transfected with sh-CAMTA1 or Ov-CAMTA1 were subcutaneously injected into mice for the establishment of MDA-MB-231 tumor-bearing nude mice model. The appearance of tumor was shown in Fig. 8B. As illustrated in Fig. 8C and D, CAMTA1 overexpression increased the tumor volume and weight, whereas CAMTA1

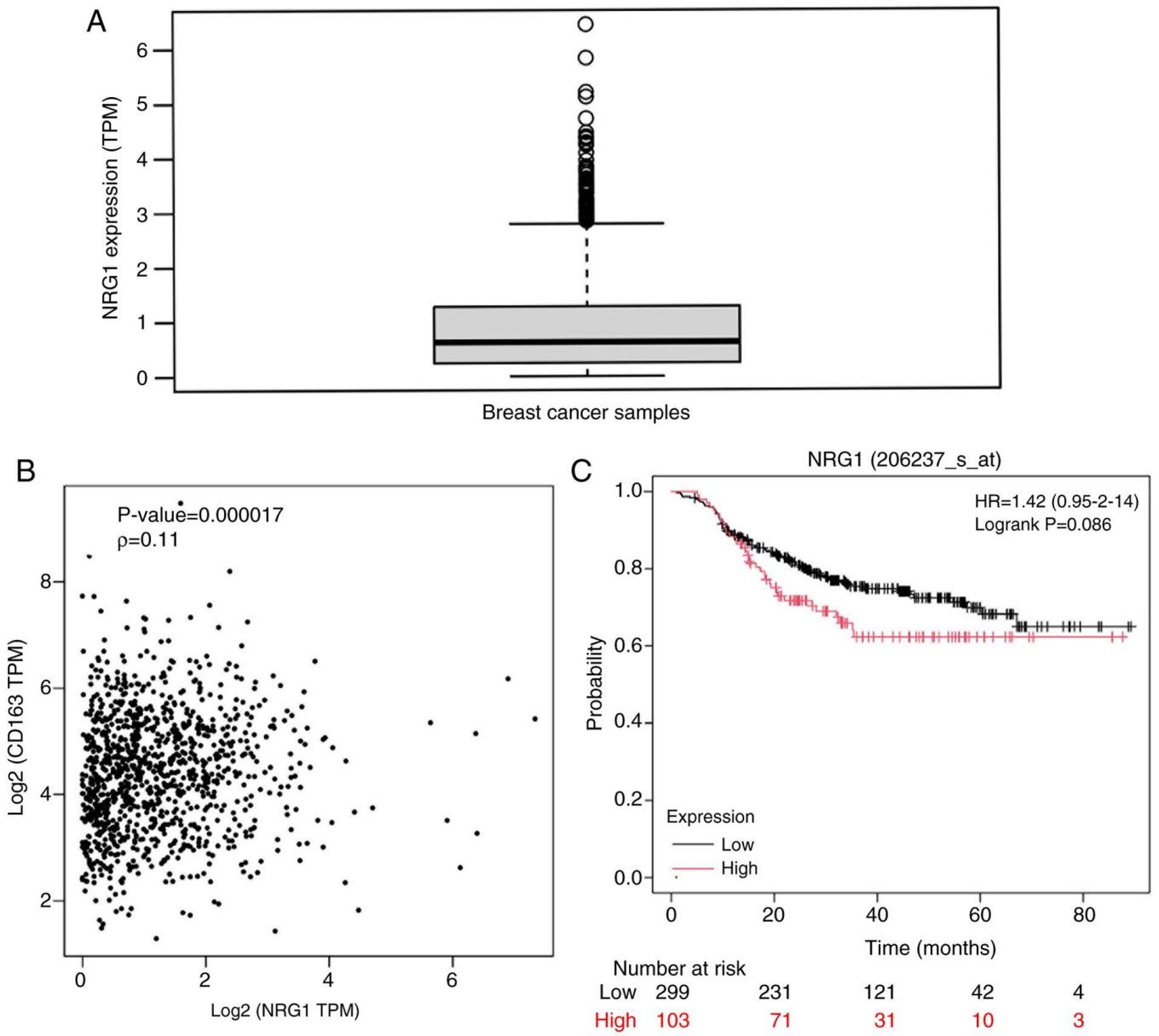

Figure 4. NRG1 expression is associated with M2 polarization and poor prognosis. (A) The expression of NRG1 in BC samples using TCGA database. (B) Spearman correlation analysis between NRG1 and CD163 expression in breast cancer samples. (C) The association of NRG1 expression with the overall survival in BC patients. NRG1, neuregulin 1; BC, breast cancer; TCGA, The Cancer Genome Atlas; GEPIA, Gene Expression Profiling Interactive Analysis.

knockdown produced the opposite effects. Throughout the present study, the maximum tumor volume measured was ~850 mm^3, with a corresponding maximum diameter of ~10 mm. RT-qPCR analysis confirmed that CAMTA1 expression in tumor tissues was elevated by CAMTA1 overexpression and reduced by CAMTA1 silencing compared with the Hypoxia exo group (Fig. 8E). Furthermore, the expression levels of IL-10 and CD163, which were elevated in the Hypoxia exo group, were further increased upon CAMTA1 overexpression, suggesting that CAMTA1 promoted M2 polarization *in vivo* (Fig. 8F and G). Additionally, CAMTA1 overexpression increased tumor cell viability and suppressed Caspase 3 expression, while CAMTA1 silencing exerted the opposite effects (Fig. 8H and I).

Correlation analysis revealed a positive association between CAMTA1 and NRG1 expression (Fig. 8J). Immunohistochemistry further confirmed that CAMTA1 overexpression markedly upregulated NRG1 expression in tumor tissues, suggesting that CAMTA1 may positively regulate NRG1 in BC (Fig. 8K).

Discussion

Hypoxia, a hallmark of the tumor microenvironment, is strongly associated with tumor progression and therapeutic resistance (27). A previous study supported that hypoxia stimulates the release of exosomes from cancer cells, which in turn promote tumor growth and survival (28). The present study isolated exosomes from hypoxia-treated MDA-MB-231 cells and investigated their role in modulating macrophage polarization and radio-resistance. The findings identified exosomal CAMTA1 as a key mediator that enhanced the radio-resistance in MDA-MB-231 cells, possible through

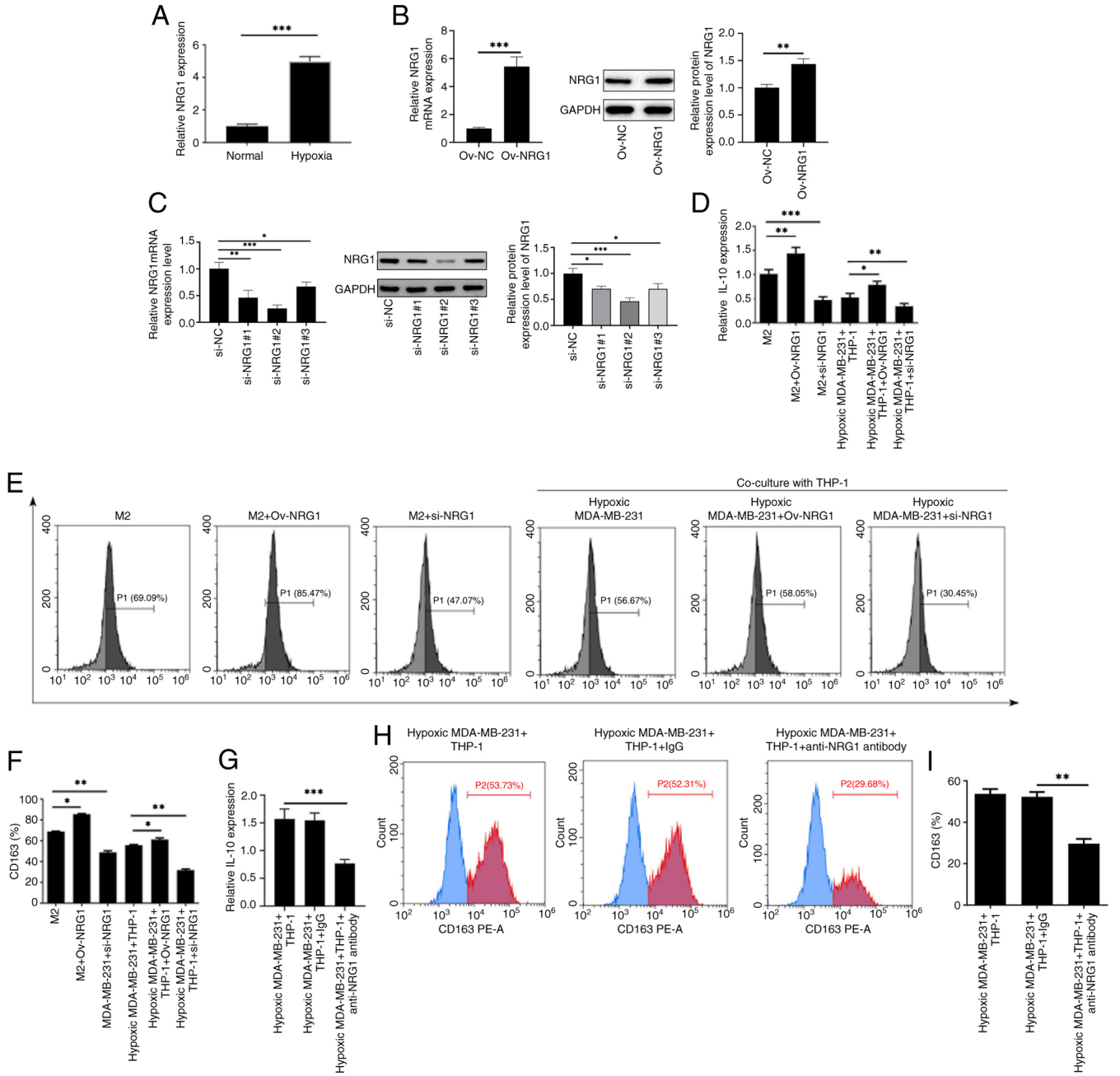

Figure 5. Hypoxic MDA-MB-231 cells induces the M2 polarization of THP-1 macrophages via NRG1. (A) The mRNA expression of NRG1 was detected using RT-qPCR. (B) The transfection efficacy of Ov-NRG1 was detected using RT-qPCR and immunoblotting analysis. (C) The transfection efficacy of si-NRG1 was detected using RT-qPCR and immunoblotting analysis. (D) The level of IL-10 was detected using ELISA-related IL-10 assay kits. (E and F) The level of CD163 was detected using flow cytometry. (G) Following the treatment of anti-NRG1 blocking antibody, the level of IL-10 was detected using ELISA-related IL-10 assay kits. (H-I) Following the treatment of anti-NRG1 blocking antibody, the level of CD163 was detected using flow cytometry. *P<0.05, **P<0.01 and ***P<0.001. NRG1, neuregulin 1; RT-qPCR, reverse transcription-quantitative PCR; Ov, overexpression; si, small interfering.

promoting M2 macrophage polarization via NRG1. The present study provided the first evidence, to the best of the authors' knowledge, linking hypoxia-driven exosomal CAMTA1 to therapeutic resistance, highlighting it as a novel therapeutic target for sensitizing BC to radiotherapy.

Exosomes are well recognized as key mediators of intercellular communication, particularly within the tumor microenvironment. It is well established that tumor-derived exosomes contribute to immunosuppression and tumor progression (21). Among immune cells, M2 macrophages play important roles in driving tumor growth and migration (29,30). For instance, bladder cancer-derived exosomes have been reported to accelerate tumor progression by stimulating M2 macrophage polarization (31). Similarly, Wang *et al* (32) demonstrated that liver cancer cells-derived exosomes under hypoxic conditions promote M2 polarization and increase tumor cell migration. Moreover, a recent study has showed that BC cell-derived exosomes can be internalized by macrophages during co-culture, thereby inducing M2 macrophage polarization and facilitating cell migration (33). Consistent with the aforementioned findings, the present results showed that hypoxic-derived exosomes from BC cells facilitated M2

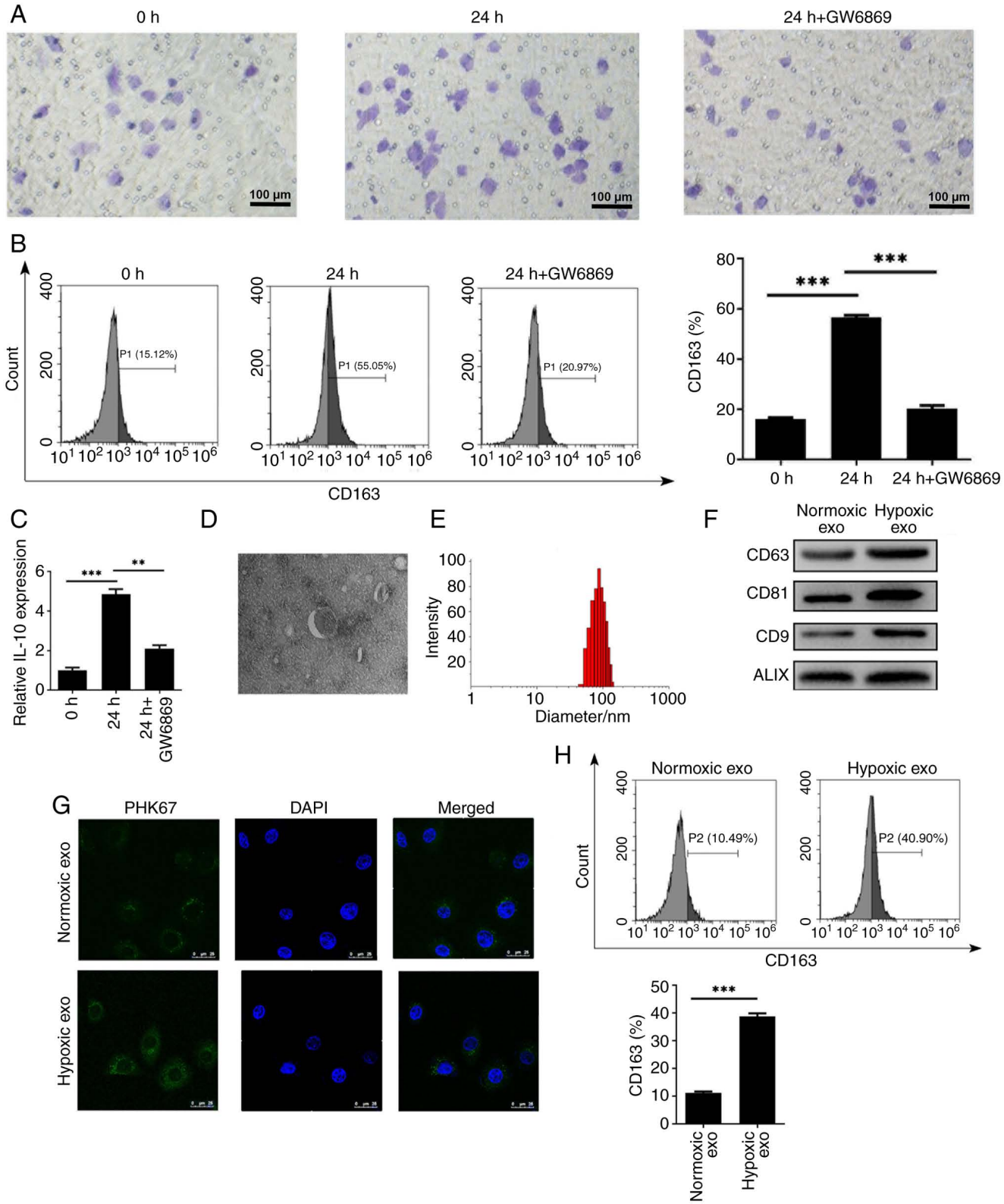

Figure 6. Hypoxic MDA-MB-231 cells mediate the M2 polarization of THP-1 macrophages via exosomes. (A) The cell migration was detected using Transwell. Scale: 100 μm. (B) The level of CD163 was detected using flow cytometry analysis. (C) The level for IL-10 was detected using ELISA-related IL-10 assay kits. (D) Transmission electron microscope was used for the inspection of exosomes. Scale: 100 μm. (E) The analysis of exosome particle size. (F) The expressions of exosomal marker proteins were detected using immunoblotting analysis. (G) PKH67 staining was used to trace the exosomes. (H) The level of CD163 was detected using flow cytometry analysis. **P<0.01 and ***P<0.001.

macrophage polarization, which in turn enhanced the proliferation and suppressed the apoptosis of BC cells expose to radiotherapy *in vitro*.

To clarify the molecular contributors to exosome-mediated polarization, the present study focused on CAMTA1, a transcriptional regulator previously implicated in tumor

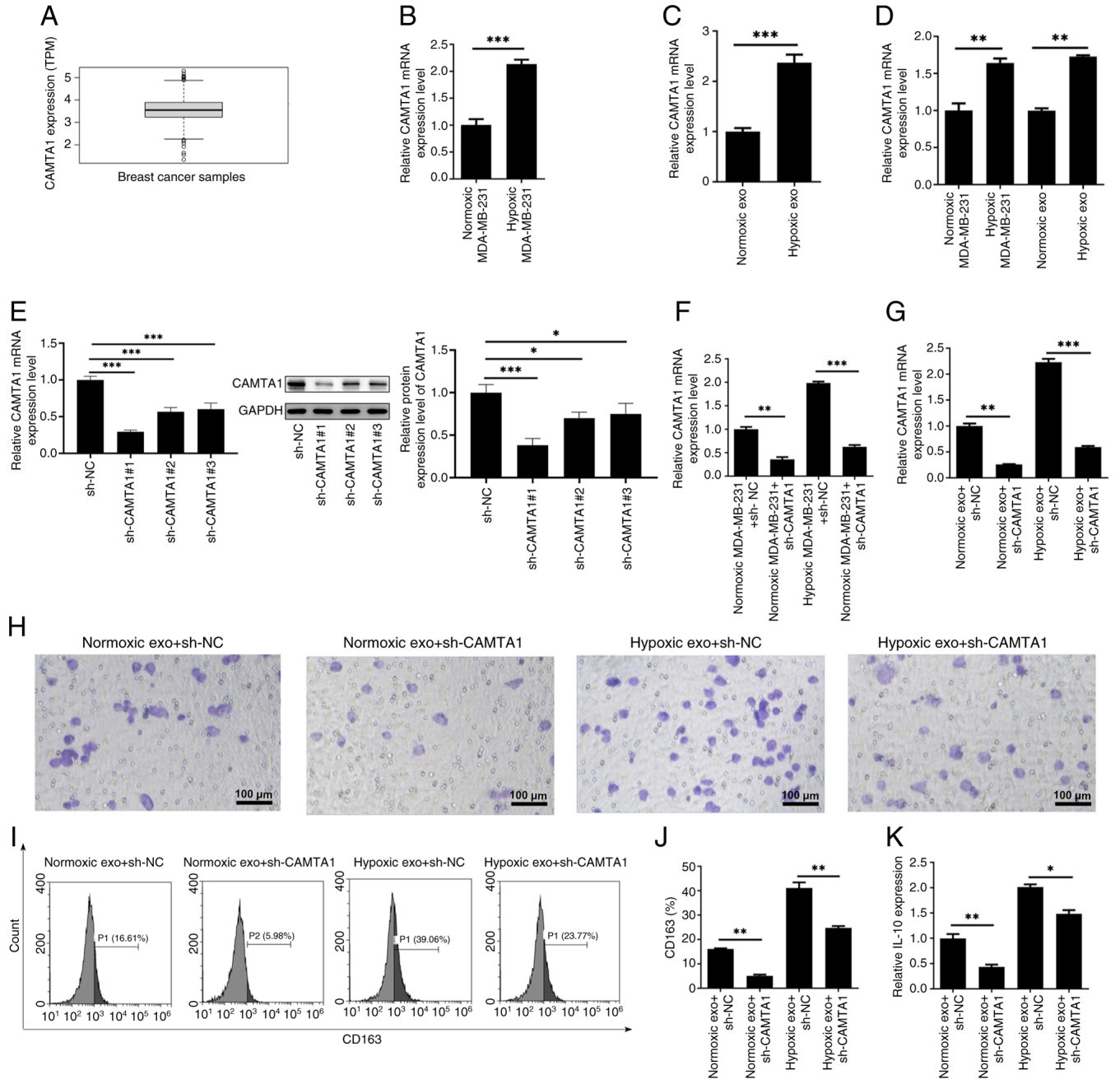

Figure 7. Exosomal CAMTA1 promotes the M2 polarization of THP-1 macrophages. (A) The expression of CAMTA1 in BC samples was predicted using TCGA database. (B) The mRNA expression of CAMTA1 in MDA-MB-231 cells was detected using RT-qPCR. (C) The mRNA expression of CAMTA1 in exosomes was detected using RT-qPCR. (D) The mRNA expression of CAMTA1 in THP-1 macrophages was detected using RT-qPCR. (E) The transfection efficacy of sh-CAMTA1 was detected using RT-qPCR and immunoblotting analysis. (F) The mRNA expression of CAMTA1 in transfected MDA-MB-231 cells was detected using RT-qPCR. (G) The mRNA expression of CAMTA1 in transfected exosomes was detected using RT-qPCR. (H) The cell migration was detected using Transwell. (I and J) The level of CD163 was detected using flow cytometry analysis. (K) The level of IL-10 was detected using ELISA-related IL-10 assay kits. *P<0.05, **P<0.01 and ***P<0.001. CAMTA1, Calmodulin-binding Transcription Activator 1; BC, breast cancer; TCGA, The Cancer Genome Atlas; RT-qPCR, reverse transcription-quantitative PCR; sh, short hairpin.

progression (11,34). Analysis of TCGA database revealed that CAMTA1 expression is markedly upregulated in BC samples. Consistently, the present study observed increased CAMTA1 expression in both hypoxic MDA-MB-231 cells and their secreted exosomes. Importantly, CAMTA1 levels were markedly increased in macrophages after co-culture with hypoxia-derived exosomes, indicating effective exosomal transfer. To determine its functional relevance, CAMTA1 was silenced in MDA-MB-231 cells, resulting in a notable reduction in both cellular and exosomal CAMTA1 levels. Furthermore, the silencing of CAMTA1 failed to induce typical M2-like phenotypes in macrophages, as evidenced by decreased migratory ability and lower CD163 expression. To our knowledge, this is the first report to identify CAMTA1 as an exosomal cargo that promotes M2 polarization and contributes to radio-resistance in BC.

Given the apparent involvement of CAMTA1 in regulating macrophage polarization, the present study next

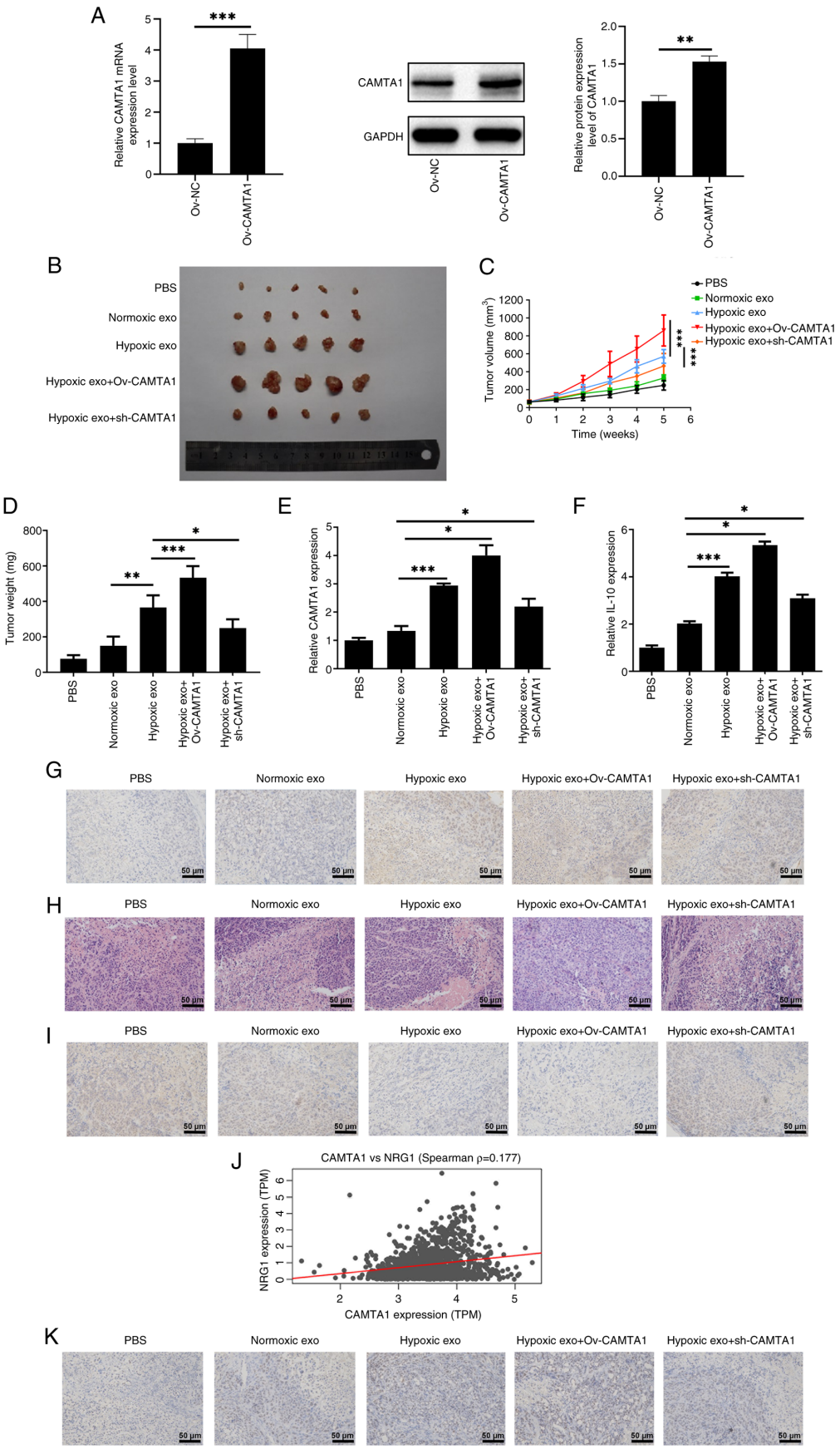

Figure 8. Exosomal CAMTA1 promotes tumor growth *in vivo*. (A) The transfection efficacy of Ov-CAMTA1 was detected using RT-qPCR and immunoblotting analysis. (B) The appearance of tumor. The tumor (C) volume and (D) weight. (E) The mRNA expression of CAMTA1 was detected using RT-qPCR. (F) The level of IL-10 was detected using ELISA-related IL-10 assay kits. (G) The level of CD163 was detected using immunohistochemistry analysis. (H) H&E staining. (I) The expression of Caspase 3 was detected using immunohistochemistry analysis. (J) The Spearman correlation analysis of CAMTA1 and NRG1. (K) The expression of NRG1 was detected using immunohistochemistry analysis. *P<0.05, **P<0.01 and ***P<0.001. CAMTA1, Calmodulin-binding Transcription Activator 1; Ov, overexpression; RT-qPCR, reverse transcription-quantitative PCR; H&E, hematoxylin and eosin; NRG1, neuregulin 1.

investigated the role of NRG1, an oncogene implicated in various malignancies. A previous study demonstrated elevated NRG1 expression in metastatic hepatocellular carcinoma cells (35) and in thyroid cancer sample tissues (36). In the present study, NRG1 expression was markedly increased in THP-1 macrophages co-cultured with hypoxia-treated MDA-MB-231 cells and RNA-seq data from RAW264.7 macrophages co-cultured with 4T1 cells further confirmed this upregulation, which was suppressed following irradiation. These findings implied that NRG1 may mediate immune-modulatory processes related to radiotherapy. Consistent with this notion, NRG1 has been shown to enhance M2 macrophage populations (37) and to promote microglia M2 polarization in neuropathic pain following spinal cord injury (38). Supporting this, GEPIA2 analysis revealed a positive correlation between NRG1 expression and the M2 marker CD163. Moreover, as IL-10 is a key cytokine characteristic of reparative M2 macrophages (39), the present study further corroborated these observations: NRG1 overexpression elevated both CD163 expression and IL-10 secretion in macrophages co-cultured with hypoxic MDA-MB-231 cells, confirming its role in promoting M2 macrophage polarization.

To substantiate these findings *in vivo*, xenograft tumor experiments were performed in mice, demonstrating that hypoxic exosomes enriched with CAMTA1 markedly promoted tumor growth of xenograft tumor mice. Functional analyses revealed that CAMTA1 overexpression elevated IL-10 and CD163 levels, enhanced tumor cell viability and inhibited cell apoptosis in xenograft tumor mice with radiation treatment, suggesting that CAMTA1 could facilitate M2 polarization and promote the radio-resistance of BC cells *in vivo*. Moreover, CAMTA1 overexpression elevated NRG1 expression in tumor tissues, indicating that CAMTA1 may act upstream of NRG1 in this regulatory axis. This observation was consistent with Spearman's correlation analysis, which revealed a positive association between CAMTA1 and NRG1 expression. These results collectively proposed a novel CAMTA1-NRG1-M2 polarization pathway that contributed to hypoxia-induced radio-resistance in BC.

In summary, the present study identifies CAMTA1 as a key regulator in hypoxia-induced exosomal communication between BC cells and macrophages. By promoting M2 macrophage polarization and upregulating NRG1 expression, CAMTA1 contributes to the development of radio-resistance in MDA-MB-231 cells. Notably, the present study was the first, to the best of the authors' knowledge, to propose and provide supporting evidence for a novel CAMTA1-NRG1-M2 polarization axis, uncovering a previously unrecognized mechanism by which exosomal CAMTA1 shapes the tumor immune microenvironment and facilitates therapeutic resistance. These findings highlighted the pivotal role of exosomal CAMTA1 in modulating macrophage behavior and suggested that targeting this pathway may represent a novel and clinically relevant strategy to enhance the efficacy of radiotherapy and improve outcomes for patients with BC.

Despite these novel insights, several limitations should be acknowledged. First, although the data suggested that CAMTA1 modulates NRG1 expression, the underlying molecular mechanism remains undefined. The use of immunohistochemistry analysis alone is insufficient to confirm a direct regulatory relationship. Further studies are needed to determine whether CAMTA1 directly binds to the NRG1 promoter or exerts its effects through indirect transcriptional regulation. Second, the clinical relevance of targeting exosomal CAMTA1 in BC has not yet been fully validated. Comprehensive mechanistic studies and preclinical/clinical evaluations, are required to clarify the translational potential of CAMTA1 as a therapeutic target. Third, although HIF-1α expression was shown to remain elevated after 24 h of co-culture with macrophages under hypoxic conditions, time points beyond 24 h was not assessed. As prolonged co-culture could potentially alter HIF-1α dynamics, this represents another limitation of the current study.

Acknowledgements

Not applicable.

Funding

No funding was received.

Availability of data and materials

The raw sequencing data generated in the present study have been deposited in the NCBI Sequence Read Archive under BioProject accession PRJNA1372921 (https://www.ncbi.nlm.nih.gov/bioproject/PRJNA1372921). Individual SRA accessions include SRR36284160 and SRR36284161: https://www.ncbi.nlm.nih.gov/sra/SRR36284160, https://www.ncbi.nlm.nih.gov/sra/SRR36284161. These datasets are currently under controlled access and will be made publicly available upon acceptance.

Authors' contributions

QL conceived the experiments. QL and MJ performed the experiments. QL, BZ, WW and LX analyzed the data. JH, HG and MD confirmed the authenticity of all the raw data. All authors read and approved the final manuscript.

Ethics approval and consent to participate

All animal experiments were approved by the Animal Ethics Committee of Jiangsu Cancer Hospital and Jiangsu Institute of Cancer Research and The Affiliated Cancer Hospital of Nanjing Medical University and conducted in compliance with the National Institutes of Health Guide for the Care and Use of Laboratory Animals (approval no. IACUC-20210216-01).

Patient consent for publication

Not applicable.

Competing interests

The authors declare that they have no competing interests.

References

1. Sung H, Ferlay J, Siegel RL, Laversanne M, Soerjomataram I, Jemal A and Bray F: Global cancer statistics 2020: GLOBOCAN estimates of incidence and mortality worldwide for 36 cancers in 185 countries. CA Cancer J Clin 71: 209-249, 2021.
2. Li T, Mello-Thoms C and Brennan PC: Descriptive epidemiology of breast cancer in China: Incidence, mortality, survival and prevalence. Breast Cancer Res Treat 159: 395-406, 2016.
3. Liyanage PY, Hettiarachchi SD, Zhou Y, Ouhtit A, Seven ES, Oztan CY, Celik E and Leblanc RM: Nanoparticle-mediated targeted drug delivery for breast cancer treatment. Biochim Biophys Acta Rev Cancer 1871: 419-433, 2019.
4. Tan C, Hu W, He Y, Zhang Y, Zhang G, Xu Y and Tang J: Cytokine-mediated therapeutic resistance in breast cancer. Cytokine 108: 151-159, 2018.
5. Nalio Ramos R, Missolo-Koussou Y, Gerber-Ferder Y, Bromley CP, Bugatti M, Núñez NG, Tosello Boari J, Richer W, Menger L, Denizeau J, *et al*: Tissue-resident FOLR2$^+$ macrophages associate with CD8$^+$ T cell infiltration in human breast cancer. Cell 185: 1189-1207.e25, 2022.
6. Pan Y, Yu Y, Wang X and Zhang T: Tumor-associated macrophages in tumor immunity. Front Immunol 11: 583084, 2020.
7. Rahal OM, Wolfe AR, Mandal PK, Larson R, Tin S, Jimenez C, Zhang D, Horton J, Reuben JM, McMurray JS and Woodward WA: Blocking Interleukin (IL)4- and IL13-mediated phosphorylation of STAT6 (Tyr641) decreases M2 polarization of macrophages and protects against macrophage-mediated radioresistance of inflammatory breast cancer. Int J Radiat Oncol Biol Phys 100: 1034-1043, 2018.
8. Finkler A, Ashery-Padan R and Fromm H: CAMTAs: Calmodulin-binding transcription activators from plants to human. FEBS Lett 581: 3893-3898, 2007.
9. Nagase T, Ishikawa K, Suyama M, Kikuno R, Hirosawa M, Miyajima N, Tanaka A, Kotani H, Nomura N and Ohara O: Prediction of the coding sequences of unidentified human genes. XIII. The complete sequences of 100 new cDNA clones from brain which code for large proteins in vitro. DNA Res 6: 63-70, 1999.
10. Henrich KO, Claas A, Praml C, Benner A, Mollenhauer J, Poustka A, Schwab M and Westermann F: Allelic variants of CAMTA1 and FLJ10737 within a commonly deleted region at 1p36 in neuroblastoma. Eur J Cancer 43: 607-616, 2007.
11. Pan R, Zhang Z, Jia H, Ma J, Wu C, Xue P, Cai W, Zhang X and Sun J: CAMTA1-PPP3CA-NFATc4 multi-protein complex mediates the resistance of colorectal cancer to oxaliplatin. Cell Death Discov 8: 129, 2022.
12. Drilon A, Somwar R, Mangatt BP, Edgren H, Desmeules P, Ruusulehto A, Smith RS, Delasos L, Vojnic M, Plodkowski AJ, *et al*: Response to ERBB3-directed targeted therapy in NRG1-rearranged cancers. Cancer Discov 8: 686-695, 2018.
13. Jonna S, Feldman RA, Swensen J, Gatalica Z, Korn WM, Borghaei H, Ma PC, Nieva JJ, Spira AI, Vanderwalde AM, *et al*: Detection of NRG1 gene fusions in solid tumors. Clin Cancer Res 25: 4966-6972, 2019.
14. Yun S, Koh J, Nam SK, Park JO, Lee SM, Lee K, Lee KS, Ahn SH, Park DJ, Kim HH, *et al*: Clinical significance of overexpression of NRG1 and its receptors, HER3 and HER4, in gastric cancer patients. Gastric Cancer 21: 225-236, 2018.
15. Shu L, Chen A, Li L, Yao L, He Y, Xu J, Gu W, Li Q, Wang K, Zhang T and Liu G: NRG1 regulates Fra-1 transcription and metastasis of triple-negative breast cancer cells via the c-Myc ubiquitination as manipulated by ERK1/2-mediated Fbxw7 phosphorylation. Oncogene 41: 907-919, 2022.
16. Yi C, Wu S, Duan Q, Liu L, Li L, Luo Y and Wang A: Ferroptosis-dependent breast cancer cell-derived exosomes inhibit migration and invasion of breast cancer cells by suppressing M2 macrophage polarization. PeerJ 11: e15060, 2023.
17. Liu C, Huang X, Li S, Ji W, Luo T, Liang J and Lv Y: M2 macrophage-derived exosomes reverse TGF-β1-induced epithelial mesenchymal transformation in BEAS-2B cells via the TGF-βRI/Smad2/3 signaling pathway. Eur J Med Res 30: 271, 2025.
18. Lu F, Ye M, Shen Y, Xu Y, Hu C, Chen J, Yu P, Xue B, Gu D, Xu L, *et al*: Hypoxic tumor-derived exosomal miR-4488 induces macrophage M2 polarization to promote liver metastasis of pancreatic neuroendocrine neoplasm through RTN3/FABP5 mediated fatty acid oxidation. Int J Biol Sci 20: 3201-3218, 2024.
19. Yang Y, Li CW, Chan LC, Wei Y, Hsu JM, Xia W, Cha JH, Hou J, Hsu JL, Sun L and Hung MC: Exosomal PD-L1 harbors active defense function to suppress T cell killing of breast cancer cells and promote tumor growth. Cell Res 28: 862-864, 2018.
20. Hansen MR, Roehm PC, Chatterjee P and Green SH: Constitutive neuregulin-1/ErbB signaling contributes to human vestibular schwannoma proliferation. Glia 53: 593-600, 2006.
21. Yang Y, Wu T, Wang Y, Luo D, Zhao Z, Sun H, Zhang M, Zhang B and Han B: Hypoxic tumour-derived exosomal miR-1290 exacerbates the suppression of CD8+ T cells by promoting M2 macrophage polarization. Immunology 173: 672-688, 2024.
22. Wang Y, Zhang J, Shi H, Wang M, Yu D, Fu M, Qian Y, Zhang X, Ji R, Wang S, *et al*: M2 Tumor-associated macrophages-derived exosomal MALAT1 promotes glycolysis and gastric cancer progression. Adv Sci (Weinh) 11: e2309298, 2024.
23. Livak KJ and Schmittgen TD: Analysis of relative gene expression data using real-time quantitative PCR and the 2(-Delta Delta C(T)) method. Methods 25: 402-408, 2001.
24. Ye M, Lu F, Gu D, Xue B, Xu L, Hu C, Chen J, Yu P, Zheng H, Gao Y, *et al*: Hypoxia exosome derived CEACAM5 promotes tumor-associated macrophages M2 polarization to accelerate pancreatic neuroendocrine tumors metastasis via MMP9. FASEB J 38: e23762, 2024.
25. Guo M, Wang R, Nie M, Zhang H, Wang C, Song C and Niu S: H3K27ac-induced RHOXF2 activates Wnt2/β-catenin pathway by binding to HOXC13 to aggravate the malignant progression of triple negative breast cancer. Cell Signal 120: 111196, 2024.
26. Jiang D, Gao X, Tan R, Liu X, Zhu Y and Zhang L: Euphorbia factor L1 suppresses breast cancer liver metastasis via DDR1-mediated immune infiltration. Aging 15: 9217-9229, 2023.
27. Schito L and Semenza GL: Hypoxia-inducible factors: Master regulators of cancer progression. Trends Cancer 2: 758-770, 2016.
28. King HW, Michael MZ and Gleadle JM: Hypoxic enhancement of exosome release by breast cancer cells. BMC Cancer 12: 421, 2012.
29. Yang Y, Jin X, Xie Y, Ning C, Ai Y, Wei H, Xu X, Ge X, Yi T, Huang Q, *et al*: The CEBPB$^+$ glioblastoma subcluster specifically drives the formation of M2 tumor-associated macrophages to promote malignancy growth. Theranostics 14: 4107-4126, 2024.
30. Sun Y, Lian Y, Mei X, Xia J, Feng L, Gao J, Xu H, Zhang X, Yang H, Hao X and Feng Y: Cinobufagin inhibits M2-like tumor-associated macrophage polarization to attenuate the invasion and migration of lung cancer cells. Int J Oncol 65: 102, 2024.
31. Jiang Z, Zhang Y, Zhang Y, Jia Z, Zhang Z and Yang J: Cancer derived exosomes induce macrophages immunosuppressive polarization to promote bladder cancer progression. Cell Commun Signal 19: 93, 2021.
32. Wang X, Zhou Y, Dong K, Zhang H, Gong J and Wang S: Exosomal lncRNA HMMR-AS1 mediates macrophage polarization through miR-147a/ARID3A axis under hypoxia and affects the progression of hepatocellular carcinoma. Environ Toxicol 37: 1357-1372, 2022.
33. Hao C, Sheng Z, Wang W, Feng R, Zheng Y, Xiao Q and Zhang B: Tumor-derived exosomal miR-148b-3p mediates M2 macrophage polarization via TSC2/mTORC1 to promote breast cancer migration and invasion. Thorac Cancer 14: 1477-1491, 2023.
34. Schraivogel D, Weinmann L, Beier D, Tabatabai G, Eichner A, Zhu JY, Anton M, Sixt M, Weller M, Beier CP and Meister G: CAMTA1 is a novel tumour suppressor regulated by miR-9/9* in glioblastoma stem cells. EMBO J 30: 4309-4322, 2011.
35. Shi DM, Li LX, Bian XY, Shi XJ, Lu LL, Zhou HX, Pan TJ, Zhou J, Fan J and Wu WZ: miR-296-5p suppresses EMT of hepatocellular carcinoma via attenuating NRG1/ERBB2/ERBB3 signaling. J Exp Clin Cancer Res 37: 294, 2018.
36. Zhang TT, Qu N, Sun GH, Zhang L, Wang YJ, Mu XM, Wei WJ, Wang YL, Wang Y, Ji QH, *et al*: NRG1 regulates redox homeostasis via NRF2 in papillary thyroid cancer. Int J Oncol 53: 685-693, 2018.
37. Alizadeh A, Santhosh KT, Kataria H, Gounni AS and Karimi-Abdolrezaee S: Neuregulin-1 elicits a regulatory immune response following traumatic spinal cord injury. J Neuroinflammation 15: 53, 2018.
38. Ma Y, Fan P, Zhao R, Zhang Y, Wang X and Cui W: Neuregulin-1 regulates the conversion of M1/M2 microglia phenotype via ErbB4-dependent inhibition of the NF-κB pathway. Mol Biol Rep 49: 3975-3986, 2022.
39. Chen X, Wan Z, Yang L, Song S, Fu Z, Tang K, Chen L and Song Y: Exosomes derived from reparative M2-like macrophages prevent bone loss in murine periodontitis models via IL-10 mRNA. J Nanobiotechnol 20: 110, 2022.